Modulation Format Recognition for Optical Signals Using Connected Component Analysis

Tianwai Bo, *Student Member, IEEE*, Jin Tang, and Chun-Kit Chan, *Senior Member, IEEE*

***Abstract*— We investigate and characterize the blind modulation format recognition method based on connected component analysis for general-purpose optical receivers. A converted binary graph is generated by projecting a part of the received data in Stokes space onto a 2-D plane. We further characterize three key parameters, namely, the threshold of density filter, the size of averaging filter, and the required number of data points for successful format recognition. In addition, we compare the computation complexity of the proposed method with other format recognition methods in Stokes space. Our results show that there exists a common set of parameters such that the proposed method can recognize a number of common optical modulation formats, proving its good robustness and practicality.**

***Index Terms*— Modulation formats, optical detection, pattern recognition.**

I. Introduction

RECENTLY, flexible and software-defined optical networks have aroused much research interests. They are equipped with fully programmable bandwidth variable transponders, where the signal's data rate and the signal's modulation format are adaptive, based on the transmission length and the channel state information. In particular, it is highly desirable to have the receivers being able to automatically recognize the modulation format of the received signal, hence the most efficient digital signal processing (DSP) algorithm can be applied to achieve the optimum detection performance.

Recently, several modulation format recognition (MFR) schemes [1]–[5] have been proposed. In [1], the polarization de-multiplexed power distribution was used to identify the signal's modulation format. However, it highly depended on the optical signal-to-noise ratio (OSNR) of the received optical signal. Thus, an additional OSNR monitoring module was required [2]. In [3], the directly detected amplitude histogram was applied to an artificial neural network (ANN) for MFR. However, it required extensive training of the ANN, especially the system impairments, including chromatic dispersion (CD) and polarization mode dispersion (PMD), were considered. In [4] and [5], the Stokes space based algorithms were promising, as they were inherently tolerant to carrier phase noise, frequency offset as well as polarization mixing. However, they were mostly based on the computation-intensive iterative K-means or expectation maximization methods, which hindered their practical implementation.

In [6], we have recently proposed a new non-iterative MFR method using very simple and common image processing technique. By projecting the received samples in three-dimensional (3-D) Stoke space onto a small-sized two-dimensional (2-D) binary image, connected component analysis (CCA) [7] was employed to recognize the signal's modulation format. The computation complexity was drastically reduced, as all required processing could be implemented with logical operations. The feasibility of this method has also been experimentally demonstrated in [6]. In this letter, we further discuss the principle of our proposed CCA-based MFR method [6], in details. Extensive characterization of the key parameters in the proposed method, namely the threshold of density filter (DF), the size of averaging filter (AF) and the number of points required, are performed under different OSNR values, via numerical simulations. The results show that there exists a common set of key parameters such that the proposed CCA-based MFR method can recognize a number of common optical modulation formats in optical transmissions. Besides, the computation complexity of the proposed method is shown to be relatively lower than that of other relevant Stokes based approaches. In general, the proposed CCA-based blind MFR algorithm is a robust and practical method in modulation format recognition for optical receivers.

II. Operation Principles

At the coherent receiver, it is common to perform analog-to-digital conversion, chromatic dispersion compensation, and timing recovery, before handling the modulation format [8]. After these pre-processing, in our proposed blind CCA-based MFR method, the dual polarization signal in Jones space is first converted to the Stokes space, by [4],

$$[s_0, s_1, s_2, s_3]^T = \left[|X|^2 + |Y|^2, |X|^2 - |Y|^2, 2\Re\left\{XY^*\right\}, 2\Im\left\{XY^*\right\}\right]^T \quad (1)$$

where X and Y represent the two orthogonal polarizations, $\Re\{\}$ and $\Im\{\}$ stand for the real and the imaginary parts of a complex number, respectively, and $[.]^{\mathrm{T}}$ is the matrix transpose operation. As the absolute phase information has been removed in the transformation, the laser frequency offset and the carrier phase noise have no effects in the Stokes space. From Eq. (1), we can conclude that the phase-shift-keying (PSK) signals distribute on the plane $s_1 = 0$ in Stokes space, as they have constant amplitudes, while the quadrature amplitude modulation (QAM) signals distribute in several discrete and symmetric planes that are parallel with

Manuscript received July 5, 2016; revised September 16, 2016; accepted October 26, 2016. Date of publication November 1, 2016; date of current version December 13, 2016. This project was supported in part by CUHK Faculty of Engineering (3132822).

The authors are with the Department of Information Engineering, The Chinese University of Hong Kong, Hong Kong (e-mail: ckchan@ie.cuhk.edu.hk).

Color versions of one or more of the figures in this letter are available online at http://ieeexplore.ieee.org.

Digital Object Identifier 10.1109/LPT.2016.2623645

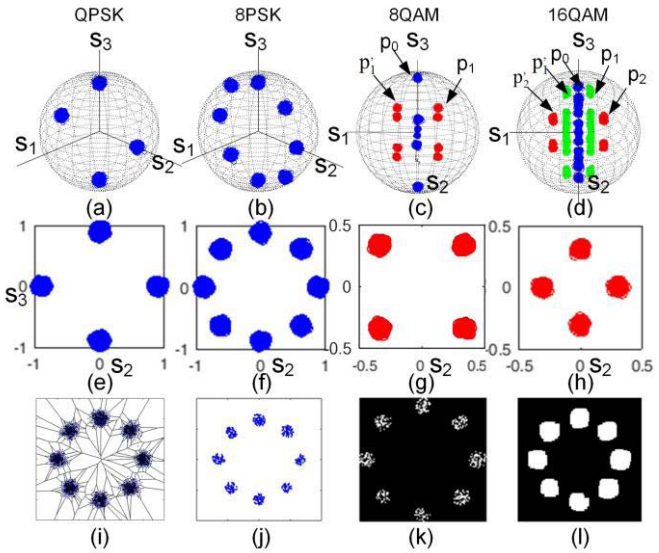

Fig. 1. Stokes representation in Poincare sphere of (a) QPSK, (b) 8-PSK, (c) 8-QAM, (d) 16-QAM, and their corresponding projections on selected planes (e)-(h); (i)Voronoi diagram of the $s_2 - s_3$ projection of a 8-PSK signal, SNR = 18 dB; (j) surviva points after density filtering; (k) converted binary graph; (l) binary graph after averaging filter.

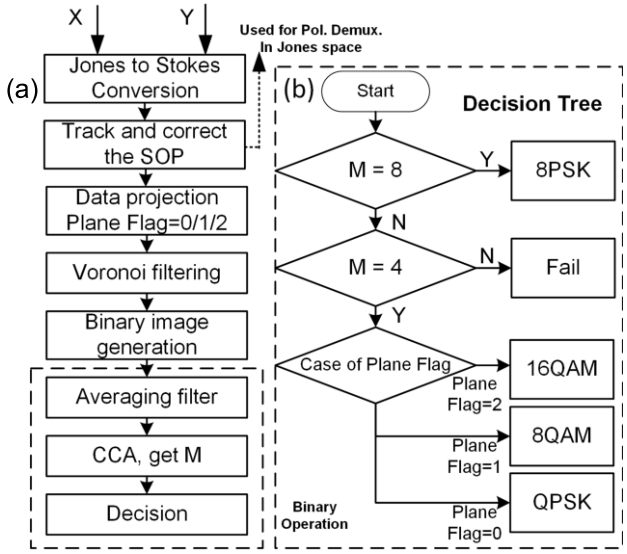

Fig. 2. (a) Flow chart of the algorithm. (b) Decision tree.

the plane $s_1 = 0$. As shown in [6], we can project the data in the outermost planes of the QAM signal (p_1 & p_1' in Fig. 1(c) and p_2 & p_2' in Fig. 1(d)) to the $s_2 - s_3$ plane ($s_1 = 0$) by their s_1 values (Fig. 1(g) and (h)), so as to increase the successful recognition rate. The 3-D distribution and the 2-D projection of the PSK-QAM signals are depicted in Figs. 1(a)-(h). As shown in Fig. 1(d), the clusters of 16-QAM signal are crowded already, hence the recognition in the Stokes space becomes very difficult for higher-order modulation formats like 32- and 64-QAM.

Fig. 2(a) illustrates the flowchart of our CCA-based MFR method. Polarization tracking is performed first, after the Stokes conversion and normalization of s_1 to s_3 values with s_0. The method proposed in [9] is employed to determine a least-square-fitting plane with only several hundreds of received data points and its normal identifies the state of polarization (SOP). A 3×3 rotation matrix is generated based on the normal of the least-square-fitting plane and it is used to recover the initial polarization of the received data. It is worth noting that simple polarization tracking does not equivalent to conventional polarization de-multiplexing because no equalization is performed. Besides, the normal can be used as the initial coefficients of the subsequent polarization de-multiplexing equalizers. Another issue to be noted is that the uncompensated PMD affects the signal quality in the Stokes space so that the compensation is required if its value is comparable as the symbol duration. Then, data slicing, based on the s_1 value of the received symbol, is performed. Only the outermost planes of the 8-QAM and the 16-QAM are selected for the projection, as in [6]. The plane flag is obtained based on the part of data chosen, and its value is 0, 1, and 2 for PSK, 8-QAM, and 16-QAM signals, respectively, so as to mark where the projected data are from. The last step of pre-processing is the Voronoi diagram based density filtering [6]. The Voronoi diagram of the points in the projected plane is generated, and the inverse of the area of each Voronoi cell is used to estimate the density of each point. After normalization of the area to be within (0, 1], a threshold is defined. The points with their estimated densities below the density threshold are removed, as seen in Fig. 1(i) & (j).

Now, it comes to the image processing process. First, a binary graph is generated with the survived points in the previous pre-processing step. The survived points are normalized with both s_2 and s_3 within (0, N], where N is an integer and defines the resolution of the generated binary image. Each data point after the density filtering is now filled in one of the $N \times N$ grids. If there is any point falling into the grid, the grid is assigned with value "1", otherwise, it is "0". This grid procedure is analogous to "quantization" in a digital communication system, and it can be easily implemented, via rounding operation of the normalized data points. Fig. 1(k) shows the binary image converted from Fig. 1(j). The second step is average filtering. It aims to smooth out the data set in the binary image and increase the recognition accuracy. It is simply a bi-directional 2-D smoothing filter implemented by two-dimensional convolution between the binary image and an $N \times N$ coefficient matrix with all coefficients being 1. Fig. 1(l) denotes the effect after applying the AF. The final step is the connected component analysis (CCA) [7]. It treats one pixel together with its adjacent 4 or 8 pixels as the connected components, as defined in Eq. (2) and Eq. (3), respectively. Here, we adopt the 8-connectivity ($N_8(p)$) as defined in Eq. (3). For each pixel, its connectivity with its neighboring pixels is first calculated, followed by the search of its connected subset. The detailed implementation of the algorithm can be found in [7], which runs in $O(n)$ time. After that, the number of the data sets, M, is used as an identifier of the individual modulation format. Fig. 2(b) illustrates the decision tree based on the number of data sets.

$$N_4(p) = \{(x \pm 1, y), (x, y \pm 1)\} \quad (2)$$

$$N_8(p) = N_4(p) \cup \{(x \pm 1, y + 1), (x \pm 1, y - 1)\} \quad (3)$$

III. Simulation Setup

In this section, we perform numerical simulations to investigate the three key parameters, mentioned above. Fig. 3

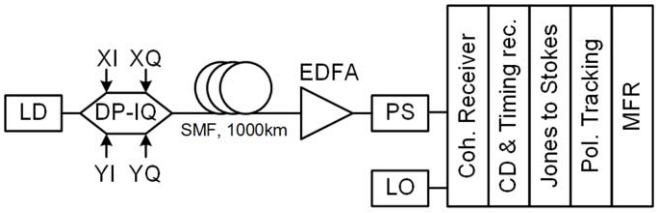

Fig. 3. Simulation setup. LD: laser diode; DP-IQ: dual-polarization in-phase/quadrature modulator; PS: polarization scrambler; Coh.: coherent; rec.: recovery; Pol.: polarization.

TABLE I
SIMULATION PARAMETERS

MF	N	OSNR (dB)	DF	AF	NS	$\lvert s_7 \rvert$
QPSK	100	12-19	0.05-1	1-20	200-10k	< 0.1
8-QAM	100	17-24	0.05-1	1-20	200-10k	0.3-0.4
8-PSK	100	21-27	0.05-1	1-20	200-10k	< 0.1
16-QAM	100	20-27	0.05-1	1-20	200-20k	> 0.4

MF: Modulation format; DF: density filter; AF: averaging filter; NS: number of symbols

shows a simplified block diagram of the system configuration. 32-Gbaud optical PM-QPSK, PM-8-PSK, PM-8-QAM and PM-16-QAM signals were generated, via a general In-phase and Quadrature (IQ) modulator. Only chromatic dispersion (D = 16 ps/nm/km) and power loss (0.2 dB/km) were taken into consideration in the fiber transmission (1000 km) model. The Erbium-doped fiber amplifiers (EDFA) module was used to adjust the signal OSNR value (normalized into 0.1nm), under the assumption of additive Gaussian white noise model. The polarization of the optical signal varied randomly to emulate polarization walk-off in the fiber. The linewidths of both the laser at the transmitter and the local oscillator were set to be 100 kHz. The carrier frequency offset between the local oscillator and the transmitter side was set to be 10 MHz. After coherent detection and digitization, the signal was converted into the Stokes space, via Eq. (1), after chromatic dispersion compensation and timing recovery. After that, our proposed CCA-based MFR method was applied.

In the simulation, 500 independent simulations for each case under investigation were tested. The success rate of format recognition was calculated so as to evaluate the effects of the individual key parameters. We have investigated the successful recognition rate with respect to the threshold of DF, the size of AF, and the number of symbols for successful recognition. In each case, a reasonable range of the OSNR values for each modulation format was considered. The forward error correction (FEC) thresholds are 12.62 dB, 17.72 dB, 17.96 dB and 19.33 dB for 32-Gbaud QPSK, 8PSK, 8QAM and 16QAM, respectively [5]. Table I lists the parameters used in the simulations.

IV. RESULTS

Fig. 4 shows the successful recognition rates of the four tested modulation formats with the threshold of DF, ranging from 0 to 1. The AF size was set to be 7 in each case. In principle, the signal at lower OSNR values required a higher DF threshold for successful recognition, as shown in Fig. 4. For each modulation format, there was a valid range

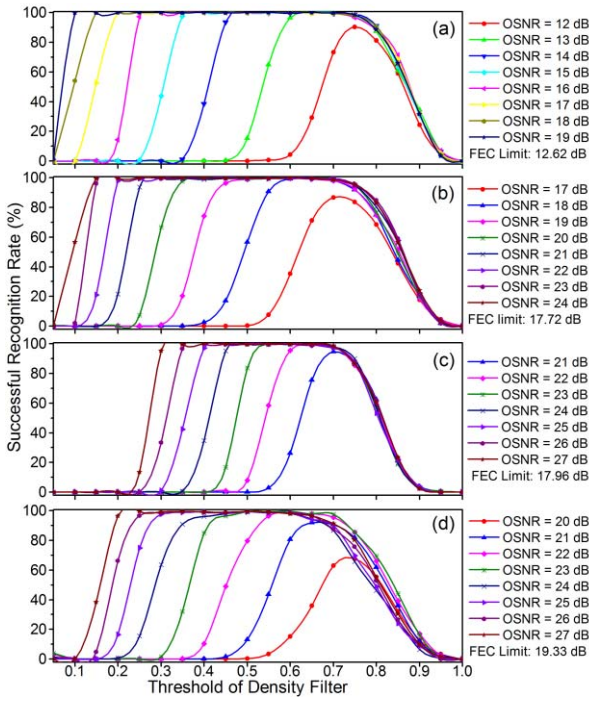

Fig. 4. Successful recognition rates w.r.t different thresholds of the density filter (DF), for (a) QPSK, (b) 8-QAM, (c) 8-PSK and (d) 16-QAM.

of DF thresholds at each OSNR value. Such valid range of DF thresholds became larger, as the OSNR increased. In general, Fig. 4 shows that there was a clear common set of DF values supporting successful recognition rates larger than 95%. Meanwhile, as seen in Fig. 5, the AF dependency of these modulation formats exhibited a similar trend. The DF threshold was set to be 0.65. The successful recognition rate at small AF size (smaller than 4 in Fig. 5) was quite low until an AF with enough size was applied. However, when the AF size was larger than a certain threshold, the CCA-based MFR method gave smaller output, as some of the subsets overlapped. This AF thresholds increased with the OSNR values, due to clearer and smaller sizes of the subsets in the binary images at higher OSNR values. These common value sets for every modulation format could be useful for practical implementation. Fig. 6 shows the required number of symbols at different OSNR values. For successful recognition rates larger than 95%, only the case of 16-QAM required more than 10000 data symbols while 3000 symbols were enough for the rest of the three modulation formats. Figs. 4-6 also show that QPSK and 8QAM could be successfully recognized as long as their OSNRs were higher than their FEC thresholds, while about 4-dB and 3-dB OSNR penalties were observed for 8PSK and 16QAM signal, respectively, due to the relatively short distances among their constellation points in the binary image. An improved OSNR sensitivity for the recognition is expected by using higher resolution of the binary image as well as advanced image processing techniques.

V. COMPLEXITY ANALYSIS

We have briefly compared the computation complexity of the proposed CCA-based MFR method with that of the K-means based algorithm. As shown in [5], K-means has

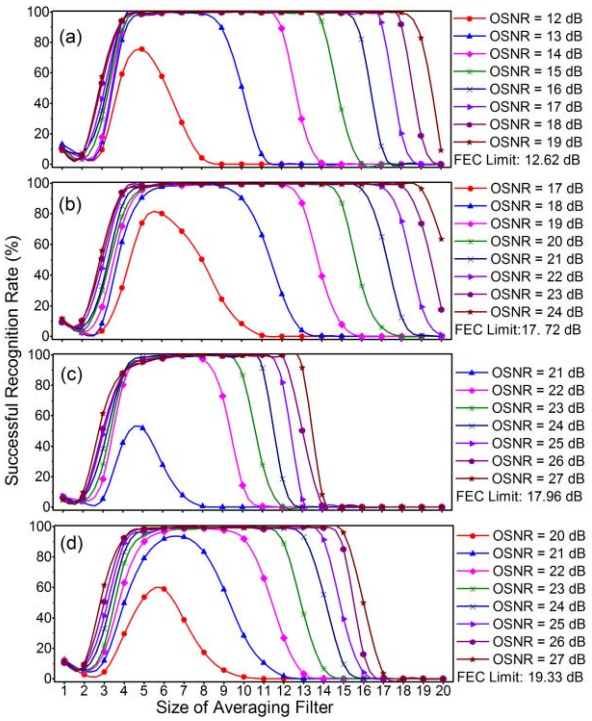

Fig. 5. Successful recognition rates w.r.t different sizes of the averaging filter(AF), for (a) QPSK, (b) 8-QAM, (c) 8-PSK and (d) 16-QAM.

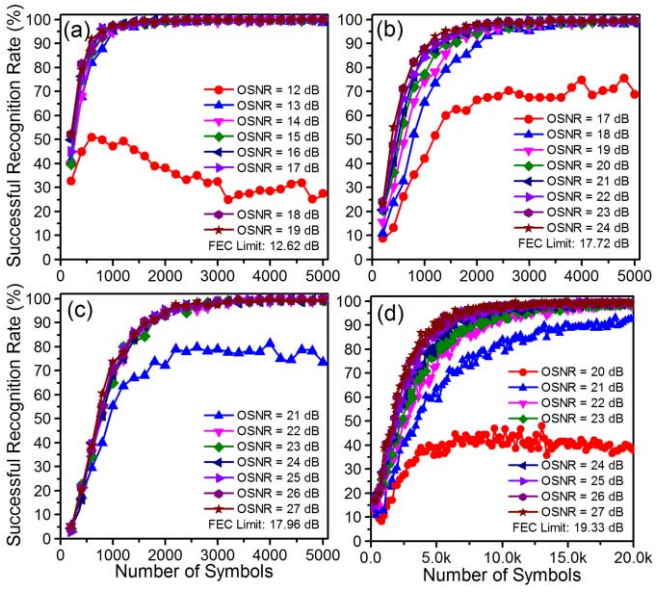

Fig. 6. Successful recognition rates under different number of symbols, for (a) QPSK, (b) 8-QAM, (c) 8-PSK and (d) 16-QAM.

smaller computation complexity than that of the expectation maximization (EM) based algorithm [4] and has comparable complexity with other machine learning algorithms. Besides, the complexity of the K-means algorithm is easy to evaluate, as the operations in each iteration mainly comprise the calculation of the Euclidean distance. In each iteration, the distance between each point to the current cluster centroid that it belongs to, is calculated, followed by updating the new centroid for each cluster at the end of the iteration. Assume the number of data symbols is N, the number of clusters is K, and I iterations are required to converge, in total. Then, about $I \times \mathrm{O}(NK + K)$ primitive operations are needed.

In our proposed CCA-based MFR method, the most computation extensive process is the Voronoi diagram generation, while the complexity of the image processing part is relatively moderate. In the well-known Fortune's algorithm [10] for Voronoi diagram calculation, there are two kinds of operations, namely site event and circle event. The number of site events is N, and that of the circle events is at most $(2N-5)$. Each event can be executed in $\mathrm{O}(\log\ N)$ time with the same number of primitive operations, in the worst case. Therefore, the total complexity is $\mathrm{O}(N \times logN)$. The area calculation is implemented in $\mathrm{O}(N)$ time. It is worth noting that the K-means algorithm is performed in 3-D space, while our proposed method employs 2-D points. Besides, the K-means algorithm needs to test every possible K value, thus the total K is 4+8+16+60=88 if only QPSK, 8-PSK, 8-QAM, and 16-QAM are considered. Considering the number of iterations, I, our non-iterative approach outperforms the K-means algorithm in the computation complexity.

VI. Summary

We have characterized the performance of our proposed CCA-based MFR method, via numerical simulations. Various key parameters, including the threshold of density filter, the size of averaging filter and the number of data samples required for successful recognition, are extensively investigated for various signal modulation formats. It is practical and simple for general coherent optical receivers.

References

[1] J. Liu, Z. Dong, K. P. Zhong, A. P. T. Lau, C. Lu, and Y. Lu, "Modulation format identification based on received signal power distributions for digital coherent receivers," in *Proc. Opt. Fiber Commun. Conf. Exhibit. (OFC)*, San Francisco, CA, USA, 2014, paper Th4D.3.

[2] S. M. Bilal, G. Bosco, Z. Dong, A. P. T. Lau, and C. Lu, "Blind modulation format identification for digital coherent receivers," *Opt. Exp.*, vol. 23, no. 20, pp. 26769–26778, Oct. 2015.

[3] F. N. Khan, Y. Zhou, A. P. T. Lau, and C. Lu, "Modulation format identification in heterogeneous fiber-optic networks using artificial neural networks," *Opt. Exp.*, vol. 20, no. 11, pp. 12422–12431, May 2012.

[4] R. Borkowski, D. Zibar, A. Caballero, V. Arlunno, and I. T. Monroy, "Stokes space-based optical modulation format recognition for digital coherent receivers," *IEEE Photon. Technol. Lett.*, vol. 25, no. 21, pp. 2129–2132, Nov. 1, 2013.

[5] R. Boada, R. Borkowski, and I. T. Monroy, "Clustering algorithms for Stokes space modulation format recognition," *Opt. Exp.*, vol. 23, pp. 15521–15531, Jun. 2015.

[6] T. Bo, J. Tang, and C.-K. Chan, "Blind modulation format recognition for software-defined optical networks using image processing techniques," in *Proc. Opt. Fiber Commun. Conf. Exhibit. (OFC)*, Anaheim, CA, USA, 2016, paper Th2A.31.

[7] A. AbuBaker, R. Qahwaji, S. Ipson, and M. Saleh, "One scan connected component labeling technique," in *Proc. IEEE Int. Conf. Signal Process. Commun.*, Nov. 2007, pp. 1283–1286.

[8] S. J. Savory, "Digital coherent optical receivers: Algorithms and subsystems," *IEEE J. Sel. Topics Quantum Electron.*, vol. 16, no. 5, pp. 1164–1179, Sep./Oct. 2010.

[9] B. Szafraniec, B. Nebendahl, and T. Marshall, "Polarization demultiplexing in Stokes space," *Opt. Exp.*, vol. 18, no. 17, pp. 17928–17939, 2010.

[10] S. Fortune, "A sweepline algorithm for Voronoi diagrams," *Algorithmica*, vol. 2, pp. 153–174, Nov. 1987.